

UBV(RI)_{KC} Photometry of NGC 2323 and NGC 2539 Open Clusters

İnci Akkaya Oralhan^{1,*}, Raúl Michel², William J. Schuster², Yüksel Karataş³, Yonca Karşlı¹ and Carlos Chavarría²

¹Erciyes University, Astronomy and Space Science Observatory, TR-38039, Kayseri, Turkey

²Observatorio Astronomico Nacional, Universidad Nacional Autonoma de México, Apartado Postal 106, C.P. 22800, Ensenada, B.C., México.

³Department of Astronomy and Space Sciences, Science Faculty, Istanbul University, 34119, Istanbul, Turkey.

*Corresponding author. E-mail: iakkaya@erciyes.edu.tr

MS received ?? ?? 2019; accepted ?? ?? 2019

Abstract. The open clusters NGC 2323 and NGC 2539 have been analysed using CCD *UBV(RI)_{KC}* photometric data, observed at the San Pedro Mártir Observatory. Cluster memberships have been determined with the proper motion and parallax measures from the GaiaDR2 astrometric data release. Photometric metal and heavy element abundances have been obtained as $([M/H], Z) = (-0.10, 0.012)$ (NGC 2323) and $(-0.31, 0.007)$ (NGC 2539), from the $\delta(U-B)$ technique in the two colour diagrams, which are used to select the appropriate PARSEC isochrones.

The estimated reddening of NGC 2323 is $E(B-V)=0.23\pm0.04$ using 11 early type stars. For NGC 2539, we find $E(B-V)=0.02\pm0.06$. For $(B-V)$ colour, distance moduli and distances for NGC 2323 and NGC 2539 are derived as $(V_0-M_V, d \text{ (pc)}) = (10.00\pm0.10, 1000\pm50)$ and $(V_0-M_V, d \text{ (pc)}) = (10.00\pm0.04, 1000\pm20)$, respectively. The median GaiaDR2 distance $d=1000\pm140$ pc ($\varpi=0.998\pm0.136$ mas) for the likely members of NGC 2323 is in concordance with its four colour photometric distances 910–1000 pc. For NGC 2539, its GaiaDR2 distance $d=1330\pm250$ pc ($\varpi=0.751\pm0.139$ mas) is close to its four colour photometric distances, 1000 pc.

Fitting the PARSEC isochrones to the colour magnitude diagrams (CMDs) gives an old age, 890 ± 110 Myr, for NGC 2539. Whereas NGC 2323 has an intermediate-age, 200 ± 50 Myr. One Red Clump/Red Giant candidate (BD-12 2380) in the CMDs of NGC 2539 has been confirmed as a member in terms of the distances $d_I=950\pm50$ pc and $d_V=910\pm90$ pc of *VI* filters within the uncertainties, as compared to the distance, 1000 ± 20 pc of NGC 2539. This giant's GaiaDR2 distance ($d=1200\pm70$ pc) is not close to these photometric distances.

Keywords. Galaxy evolution—open clusters and associations, individual—Hertzsprung-Russell and C-M diagrams.

1. Introduction

CCD *UBV(RI)_{KC}* photometric data which include the *U* filter for open clusters (OCs) are quite valuable for determining the interstellar reddening, $E(B-V)$ and the photometric metallicity and heavy-element abundance $([M/H], Z)$ on colour-colour diagram (CC). The two parameters are vital importance for deriving the distance modulus, (V_0-M_V) and the distance, d (kpc) and age, A (Gyr) from colour-magnitude diagrams (CMDs).

In this study we have analysed the deep CCD *UBV(RI)_{KC}* photometry of the OCs, NGC 2323 and NGC 2539 from the Sierra San Pedro Mártir National Astronomical Observatory (SPMO) open cluster survey (cf. Schuster *et al.* 2007; Tapia *et al.* 2010 (T10); Akkaya *et al.* 2010 (A10); Akkaya Oralhan *et al.* 2015

(A15). Both OCs are uniformly and homogeneously analysed with regards to the instrumentation, observing techniques, and reduction and calibration methods. The two OCs which are located in 3rd quadrand have no spectroscopic metal abundances in the literature. Their basic parameters from the literature (Kharchenko *et al.* 2013) are listed in Table 1. NGC 2323 has been studied by Sharma *et al.* (2006) using CCD *UBVI* photometry and by Claria *et al.* (1998) from photoelectric *UBV* photometry. For NGC 2539, Choo *et al.* (2006) used CCD *UBVI* photometry to search variable stars. Joshi and Sagar (1986) studied its photoelectric *UBV* photometry. Claria and Lapsset (1986) use CCD *DDO* and *CMT₁T₂* photometries for this OC. Many published works of these OCs (Table 11) are of the brighter stars, which are based on old photographic and photoelectric

Table 1. The central equatorial (J2000) and Galactic coordinates plus the average μ_α and μ_δ values together with their standard deviations of Kharchenko *et al.* (2013). Our findings from the GaiaDR2 data are given in parentheses.

Cluster	NGC 2323	NGC 2539
α_{2000} (h m s)	07 02 43.1 (07 02 51.6)	08 10 40.8 (08 10 42)
δ_{2000} ($^\circ$ ' '')	-08 22 12 (-08 20 42)	-12 50 24 (-12 50 31)
ℓ ($^\circ$)	221.66	233.73
b ($^\circ$)	-1.33	11.11
μ_α (mas yr $^{-1}$)	+0.50 \pm 0.17 (-0.816 \pm 0.248)	-2.28 \pm 0.19 (-2.347 \pm 0.181)
μ_δ (mas yr $^{-1}$)	-1.75 \pm 0.17 (-0.653 \pm 0.210)	-1.91 \pm 0.19 (-0.569 \pm 0.205)

photometries.

Additionally, we use the GaiaDR2 astrometric data (proper motion components and parallaxes) (Gaia Collaboration, Brown *et al.* 2018) for determining the probable members for NGC 2323 and NGC 2539. The membership determinations of previous works have been based on the proper motions (*PPMXL*) of Roeser *et al.* (2010) in combination with 2MASS JHK_s values of Skrutskie *et al.* (2006). Cantat-Gaudin *et al.* (2018) state that the proper motion uncertainties of UCAC4 fall in the range of 1-10 mas yr $^{-1}$ (Roeser *et al.* 2010; Zacharias *et al.* 2013), whereas the ones of Tycho-Gaia Astrometric Solution (TGAS) (Gaia Collaboration, Brown *et al.* 2016) have the range of 0.5-2.6 mas yr $^{-1}$.

Because of the above-mentioned scientific grounds, we combine the recent GaiaDR2 astrometric data with deep CCD *UBV(RI)_{KC}* photometry of both OCs, to derive their reddenings, metal abundances, distance moduli and distances, and ages for four colour indices, (B-V), (V-I), (R-I) and (*G_{BP}*-*G_{RP}*). This kind of photometric data are also valuable for classifying early-type stars, blue stragglers, and RC/RG candidates in the CMDs, and thus possible candidates are proposed for spectroscopic observations.

This paper is organized as follows: Section 2 describes the observation and reduction techniques. The technique for determining cluster membership is presented in Section 3. Section 4 describes general procedures concerning the derivation of astrophysical parameters, and in Section 5 the results for these astrophysical parameters are presented. Discussions and Conclusions are given in Section 6.

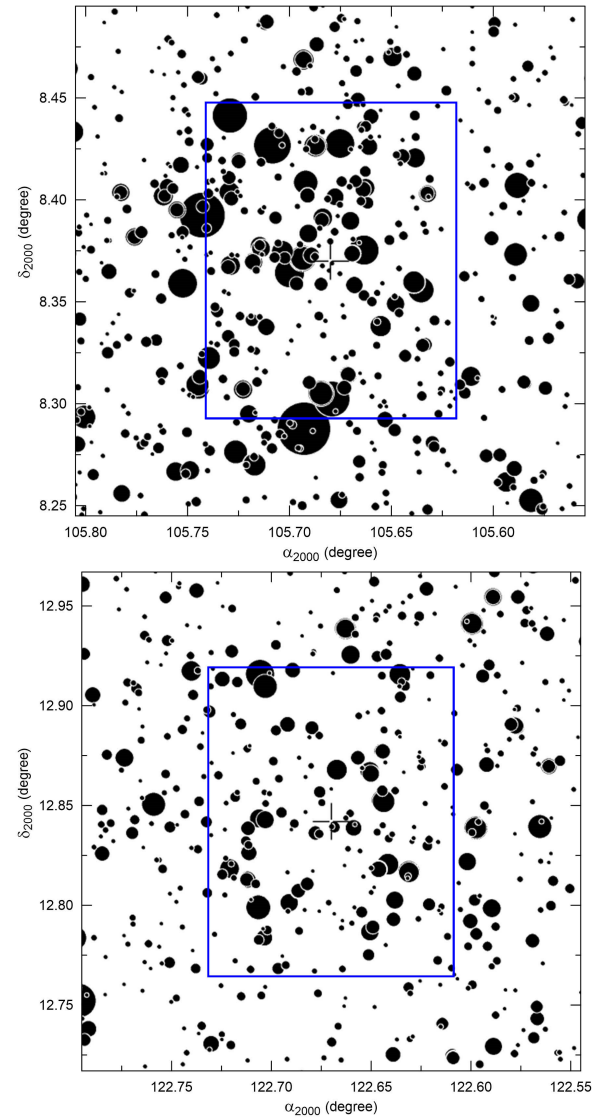


Figure 1. The images of <https://www.aavso.org> (AAVSO) of NGC 2323 (18.3'x17.23') and NGC 2539 (15.0'x 14.33'), are shown from top to bottom, respectively. The blue rectangles indicate the field of view of the SPMO detector, 7.4' \times 9.3'.

2. Observations and reductions

Observations were carried out at the SPMO, during photometric nights, on June 7-10, 2013 UT using the 0.84-m (f/15) Ritchey-Chretien telescope equipped with the Mexman filter wheel and the ESOPO CCD detector, a 2048x4608 13.5- μ m square-pixel e2v CCD42-90 with a gain of 1.7 e $^-$ /ADU and a readout noise of 3.8 e $^-$ at 2 \times 2 binning. The combination of the telescope and detector ensures an unvignetted field of view of 7.4 \times 9.3 arcmin 2 . Each OC was observed through John-

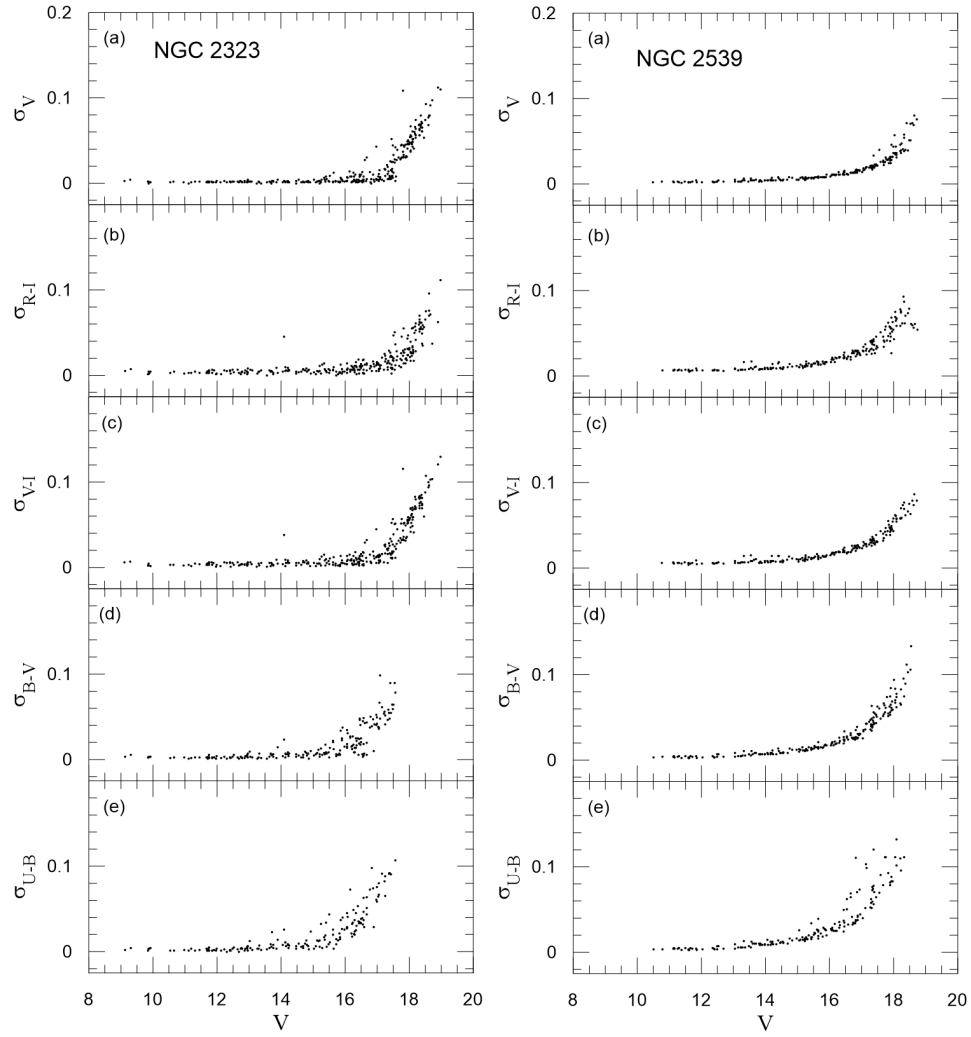


Figure 2. Photometric errors for the V magnitude and several broad-band colours plotted against the V magnitudes of NGC 2323 and NGC 2539.

Table 2. The observed open clusters and standard-star Landolt fields.

Cluster	RA (2000)	DEC (2000)	LJD (days)	Air mass range	Filter U Exp. Time (s)	Filter B Exp. Time (s)	Filter V Exp. Time (s)	Filter R Exp. Time (s)	Filter I Exp. Time (s)
NGC 2323	07:02:52.4	-08:21:01.2	2452669	1.352-1.382	60,300	10,30	6,20	4,15	4,15
NGC 2539	08:10:43.4	-12:51:41.9	2452669	1.414-1.423	300	60	25	10	8
PG0918+029	09:21:32.6	+02:47:42.9	2452669	1.135-1.136	300	220	120	80	80
RU 149	07:24:15.5	-00:32:58.0	2452669	1.174-1.175	300	65	45	50	50
RU 152	07:29:58.4	-02:06:11.2	2452669	1.198-1.523	2x300	45,50	25,27	15,16	15,18

Table 3. Coefficients of the transformation equations.

index	First Pass					Second Pass				
	z	k	c	rms	points	c	p	q	rms	points
UUB	4.188±0.022	0.417±0.016	-0.082±0.009	0.018	50	-0.144±0.050	0.031±0.039	0.010±0.015	0.022	291
UUV	4.198±0.024	0.428±0.017	-0.049±0.006	0.020	56	-0.072±0.016	0.014±0.012	0.001±0.002	0.021	301
BUB	2.527±0.018	0.206±0.013	-0.032±0.007	0.013	50	-0.104±0.055	0.014±0.043	0.047±0.015	0.023	291
BBV	2.571±0.019	0.194±0.013	-0.052±0.010	0.014	56	-0.111±0.021	0.033±0.016	0.008±0.007	0.021	355
VBV	2.189±0.019	0.118±0.013	0.067±0.010	0.014	56	0.033±0.020	0.012±0.015	0.012±0.007	0.020	355
VVR	2.170±0.021	0.131±0.015	0.122±0.022	0.017	66	0.118±0.031	-0.015±0.023	0.014±0.013	0.021	427
RVR	2.254±0.021	0.077±0.015	0.036±0.021	0.016	66	-0.002±0.032	0.013±0.025	0.029±0.014	0.022	427
RRI	2.226±0.014	0.091±0.011	0.065±0.010	0.010	56	0.081±0.033	-0.015±0.025	-0.009±0.010	0.021	388
IVI	2.547±0.027	0.004±0.018	-0.047±0.015	0.018	52	-0.084±0.019	0.036±0.014	-0.010±0.003	0.024	368
IRI	2.532±0.028	0.021±0.020	-0.116±0.017	0.022	56	-0.141±0.038	0.025±0.029	-0.009±0.011	0.025	388

Table 4. Observed standard stars (first three rows) and the subset of extinction stars (three rows at the bottom).

HJD	Meas.&(B-V)&Air Mass	Landolt Fields
2452668	596; -0.284–1.605; 1.19–1.34	PG1047+003 0035 CL13 RU149 0538 CL13
2452669	606; -0.284–1.727; 1.14–1.50	G3061911464112566400RM PG0918+029 0068 CL13 PG1047+003 0035 CL13 RU149 0525 CL13 RU152 0561 CL13
All	1202; -0.284–1.727; 1.14–1.50	
HJD	Meas.&(B-V)& Air Mass	Landolt Fields
2452668	184; -0.034–1.170; 1.19–1.34	RU149 0557 CL13
2452669	96; 0.043–1.528; 1.20–1.50	G3061911464112566400RM RU152 0586 CL13
All	96; 0.043–1.528; 1.20–1.50	

son's *UBV* and Kron-Cousin's *RI*¹ filters with short and long exposure times in order to properly record both the brighter and fainter stars of the fields under study. Standard fields (Landolt 2009) were also observed near the meridian and at 1.14–1.52 air masses to properly determine the atmospheric extinction coefficients and the equations to transform the instrumental data to the standard system. Flat fields were taken nightly at the beginning and/or the end of the night, whereas biases were recorded between cluster observations. For more details see the works of T10 and A10. The log of the observations is shown in Table 2. It contains the object names, coordinates at the centres of the observed fields, local Julian date of the observations, air-mass range during the observations, and exposure times in each band. The second part of Table 2 contains data of the observed standard fields.

The data reduction was carried out by R. Michel² using the IRAF³ package and together with some home-made auxiliary Fortran programs and Awk scripts. The supervised-automatic procedure, implemented by C. Chavarria, can be condensed as follows. All the images were bias subtracted and flat-field corrected (CCDRED); cosmic rays were then removed with the L.A. Cosmic⁴ script (van Dokkum 2001).

The images of each set of observations were aligned and trimmed (IMALIGN), generating a template image of each cluster field (IMSUM). By using these template images, in addition to reference images from the ESO

Digital Sky Survey⁵, and equatorial coordinates from the 2MASS All-Sky Catalog of Point Sources (Cutri *et al.* 2003), an astrometric solution is obtained (CCMAP and CCTRAN) providing a means to transform pixel coordinates to equatorial coordinates of each detected star.

For each image, the average sky level and its standard deviation are iteratively calculated with the help of the IMSTAT routine. The average *FWHM* of the stars in each image is also found by means of DAOFIND, FITPSF, and filtering routines. With this information, bright-unsaturated-isolated stars are identified and used iteratively to build the point spread function (PSF) for each image. Consequently, instrumental magnitudes are calculated using the ALLSTAR routine (Stetson 1987).

The aperture photometry (PHOT) of the standard stars was calculated using a fixed aperture radius of $2(FWHM + 3\sigma)$ where *FWHM* was the average *FWHM* of the run, and σ its standard deviation. The pixel coordinates of each measured star are then transformed to their corresponding equatorial coordinates. The standard magnitudes were taken from the catalogue by Landolt (2009) and supplemented with the secondary photometric standards by Cutri *et al.* (2013). As a result, the transformation coefficients were found (FITPARAMS) using Equations 1–10:

$$u = U + z_{UUB} + k_{UUB}X_U + c_{UUB}(U - B) + p_{UUB}X_U(U - B) \quad (1)$$

$$u = U + z_{UUV} + k_{UUV}X_U + c_{UUV}(U - V) + p_{UUV}X_U(U - V) \quad (2)$$

$$b = B + z_{BUB} + k_{BUB}X_B + c_{BUB}(U - B) + p_{BUB}X_B(U - B) \quad (3)$$

$$b = B + z_{BBV} + k_{BBV}X_B + c_{BBV}(B - V) + p_{BBV}X_B(B - V) \quad (4)$$

$$v = V + z_{VUV} + k_{VUV}X_V + c_{VUV}(U - V) + p_{VUV}X_V(U - V) \quad (5)$$

$$v = V + z_{VVR} + k_{VVR}X_V + c_{VVR}(V - R) + p_{VVR}X_V(V - R) \quad (6)$$

$$r = R + z_{RVR} + k_{RVR}X_R + c_{RVR}(V - R) + p_{RVR}X_R(V - R) \quad (7)$$

$$r = R + z_{RRI} + k_{RRI}X_R + c_{RRI}(R - I) + p_{RRI}X_R(R - I) \quad (8)$$

$$i = I + z_{IVI} + k_{IVI}X_I + c_{IVI}(V - I) + p_{IVI}X_I(V - I) \quad (9)$$

$$i = I + z_{IRI} + k_{IRI}X_I + c_{IRI}(R - I) + p_{IRI}X_I(R - I), \quad (10)$$

where *u*, *b*, *v*, *r*, *i* are the magnitudes in the instrumental system, *U*, *B*, *V*, *R*, *I* the magnitudes in the standard system, and *X* is the air mass during the measurement. During the first iteration, only the first-order extinction measurements (for the stars observed over an extended range of air mass) were used to calculate the zero point (*z*), first-order extinction (*k*), and colour (*c*) coefficients; the second-order extinction (*p*) was zeroed. For the second iteration, all data were used, having the zero points and first-order extinction values fixed to the values found in the previous iteration, while the colour-dependent coefficients (*p* and *c*) were re-calculated. *p* corrects the shift in λ_{eff} due to the convolution of the spectral-energy distribution of the stars with the wavelength dependence of *k*. These values are given in Table 3.

¹personel communication of A. Landolt.

²Data may be requested from R. Michel.

³IRAF is distributed by the National Optical Observatories, operated by the Association of Universities for Research in Astronomy, Inc., under cooperative agreement with the National Science Foundation.

⁴<http://www.astro.yale.edu/dokkum/lacosmic>

⁵<http://archive.eso.org/dss/dss>

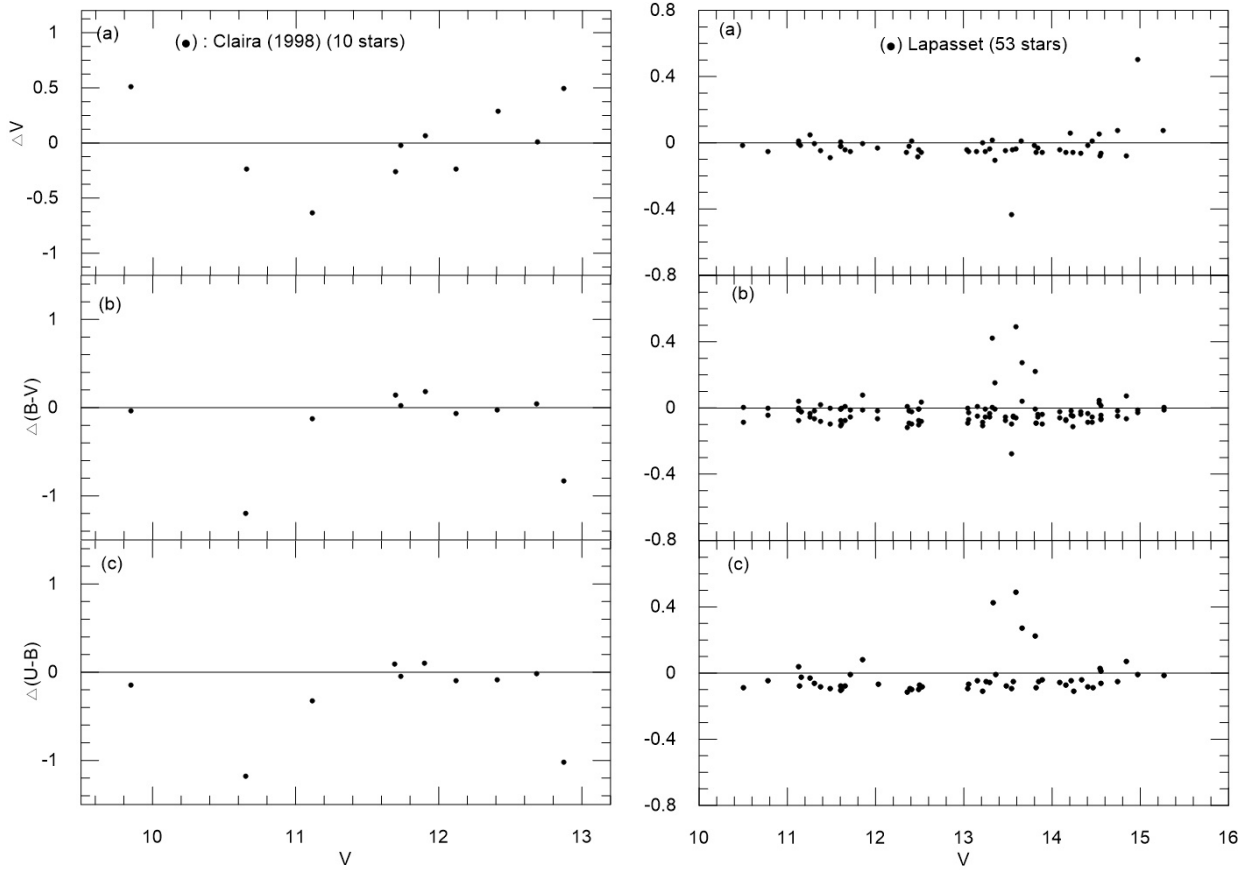


Figure 3. For NGC 2323 (left panels) and NGC 2539 (right panels), comparisons of the present CCD photometry with data from the literature: Clairia *et al.* (1998) and Lapasset *et al.* (2000), respectively. The difference Δ (present photometry minus literature values) as a function of the V mag.

Table 5. The mean photometric errors of V , $(R-I)$, $(V-I)$, $(B-V)$, and $(U-B)$ for NGC 2323 and NGC 2539 in terms of the V mag.

V	σ_V	σ_{R-I}	σ_{V-I}	σ_{B-V}	σ_{U-B}
NGC 2323					
9-10	0.002	0.004	0.004	0.003	0.003
10-11	0.001	0.003	0.003	0.002	0.001
11-12	0.001	0.004	0.004	0.002	0.002
12-13	0.002	0.004	0.004	0.003	0.003
13-14	0.002	0.004	0.004	0.005	0.007
14-15	0.002	0.006	0.005	0.005	0.009
15-16	0.003	0.006	0.006	0.012	0.018
16-17	0.007	0.009	0.011	0.025	0.041
17-18	0.024	0.020	0.030	-	-
18-19	0.064	0.050	0.074	-	-
NGC 2539					
10-11	0.003	0.006	0.005	0.004	0.004
11-12	0.002	0.007	0.006	0.004	0.004
12-13	0.003	0.006	0.006	0.005	0.005
13-14	0.004	0.009	0.008	0.007	0.008
14-15	0.005	0.010	0.009	0.009	0.012
15-16	0.007	0.014	0.012	0.014	0.021
16-17	0.013	0.024	0.021	0.025	0.039
17-18	0.022	0.041	0.037	0.051	0.077
18-19	0.040	0.067	0.065	0.085	0.110

For the case of this observing run, the number of valid measurements used in the transformations is shown in first three rows of Table 4 together with the colour and air-mass range near zenith of the standard fields. Table 4 includes the local Julian date of the observations, the number of measurements, the interval of the colour ($B-V$), the air-mass range, and Landolt's field name. The resulting coefficients found using Equations 1–10, the *rms* deviations of the fits, and the number of stars used in the calculations are given in three rows at the bottom of Table 4. New images that contained only the PSF stars were generated with the help of the GROUP, NSTAR and SUBSTAR routines, and aperture corrections were calculated with PHOT and MKAPFILE of IRAF. The mean value of the aperture correction is about -0.2 magnitude.

Fig. 1 presents finding charts ⁶ The blue rectangles indicate the analysed regions of these OCs, the field of view of the SPMO detector, $7.4' \times 9.3'$.

⁶Obtained from <https://www.aavso.org> (AAVSO) web page of NGC 2323 ($18.3' \times 17.23'$) and NGC 2539 ($15.0' \times 14.33'$).

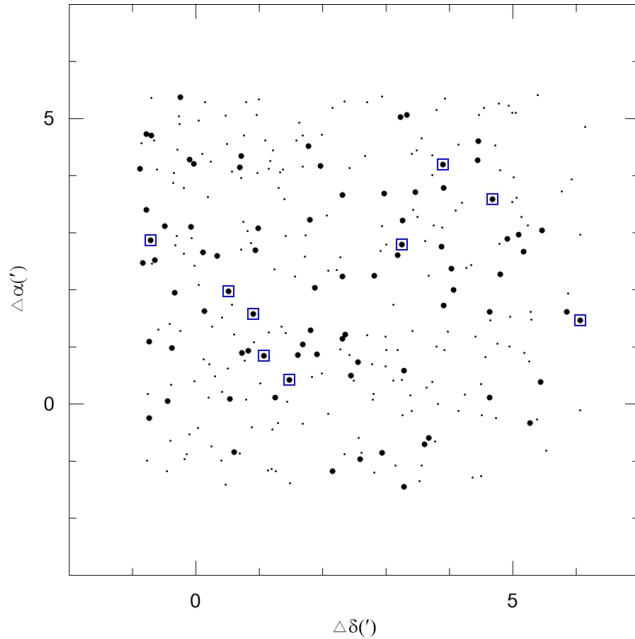


Figure 4. The finding chart is presented for NGC 2323 only. The size of filled dots for our CCD UBVI photometry is proportional to the magnitudes of stars: $V = 9 - 15$ mag, large dots, and $15 - 19$ mag, small dots. The blue squares show stars with photoelectric photometry of Claria *et al.* (1998) for $V < 13.00$. $\Delta\alpha$ and $\Delta\delta$ are in units of arcmin, and are measured from the cluster center of NGC 2323 in WEBDA.

The photometric errors in V and colours ($R-I$), ($V-I$), ($B-V$), ($U-B$) of NGC 2323 (left panel) and NGC 2539 (right panel) are presented in Fig. 2. Their mean errors are listed in Table 5. Our inspection of Fig. 2 and Table 5 indicates that stars brighter than $V \approx 17^m.00$ have errors smaller than $\approx 0^m.05$ in both magnitudes and colours. For $V > 17^m.00$, large errors in ($U-B$) dominate. The stars with $V < 17^m.00$ have been considered for our analyses.

A comparison of the present data with those in the literature for stars in common is done in Fig. 3 for NGC 2323 (left panels) and NGC 2539 (right panels). For the comparisons, we have considered only photoelectric photometry from the literature. For this purpose, a finding chart is shown in Fig. 4 for NGC 2323. The size of filled dots for our CCD UBVI photometry is proportional to the magnitudes of stars: $V = 9^m.0 - 15^m.0$ (large dots) and $15^m.0 - 19^m.0$ (small dots). The blue squares show stars with the photoelectric photometry of Claria *et al.* (1998) for $V < 13^m.0$. From the left panels of Fig. 3 (for 10 stars in common), our magnitudes and colours, V , ($U-B$), and ($B-V$), do not show any systematic trends with the photoelectric data of Claria *et al.* (1998). Three stars with up to $\Delta V = 0^m.50$

are seen in panel (a), and two stars with large color deviations in $\Delta(U-B)$ and $\Delta(B-V)$, at $V = 10^m.65$ and $V = 12^m.87$, in panels (b)-(c) of Fig. 3. The magnitudes and colours of Claria *et al.* (1998) are somewhat fainter and redder than our CCD UBVI photometry.

For NGC 2539, the comparison with the photoelectric data of Lapasset (2000) is done for 53 stars in common in the right panels of Fig. 3. For $V = (13^m.0, 14^m.0)$, differences up to $0^m.40$ in ($B-V$) and ($U-B$) for a few stars indicate that our photometry gives bluer colours than the ones of Lapasset (2000); these 4–5 deviating stars are not easily explained, not by cosmic rays or cosmetic effects in the CCD data, but perhaps by stellar variability or typographical errors of Lapasset (2000).

3. Cluster Membership

For the separation of the likely cluster members of NGC 2323 and NGC 2539, firstly, CCD $UBVI(RI)_{KC}$ photometric data of NGC 2323 (170 stars) and NGC 2539 (155 stars) have been matched with the GaiaDR2 astrometric data (proper motions and parallaxes) from SIMBAD-VizieR⁷. GaiaDR2 astrometric and photometric data of the field stars in a region of $R = 20$ arcmin centered on our target OCs have also been considered to determine the cluster's radii. The μ_α versus μ_δ (Vector Point Diagram, VPD) of the two OCs are plotted in top panels of Fig. 5 for both the background/foreground field stars (small grey dots) and our OCs (filled dots). The proper motion radii (shown with blue circles) of 0.6 mas yr^{-1} around the centres of their VPDs define the membership criteria. These proper motion radii have been empirically fitted until the likely members inside these radii provide good single stellar sequence on G , $G_{BP}-G_{RP}$ and V , ($B-V$) plots (bottom panels of Fig. 5). Therefore, the chosen radii are a good compromise for the likely cluster members. These proper motion radii have been constructed via the mathematical equations, $x = x_0 + r \cos(\theta)$ and $y = y_0 + r \sin(\theta)$. Here, (x_0, y_0) are the median values of (μ_α, μ_δ) (mas yr^{-1}), the radius $r = \sqrt{\sigma_{\mu_\alpha}^2 + \sigma_{\mu_\delta}^2}$ mas yr^{-1} , and $\theta = 0^\circ$ to 360° . Note that there almost seems to be a clear concentration of stars inside the chosen proper motion radii. The inset plots (Fig. 5) show the likely cluster members inside the proper motion radii of NGC 2323 (74 probable members) and NGC 2539 (67 probable members). The big red pluses indicate the median values of proper motion components of the two OCs.

⁷<http://vizier.u-strasbg.fr/viz-bin/VizieR>

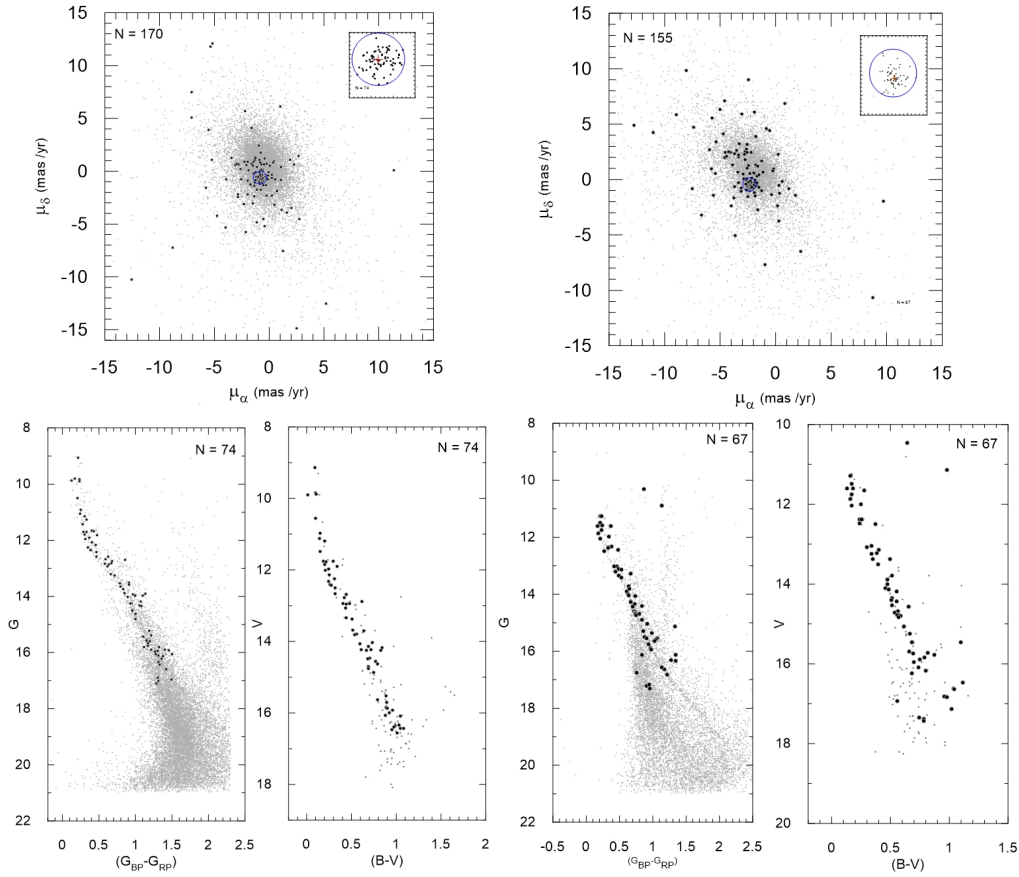


Figure 5. The μ_α versus μ_δ for NGC 2323 (left, top panel) and NGC 2539 (right, top panel). Small dots represent the GaiaDR2 astrometric and photometric data for a 20 arcmin region centered on the two OCs. Blue circles denote the radii of 0.6 mas yr⁻¹. The likely members inside the blue circles are also indicated in the inset of the top panels. The big red pluses indicate the median proper motions of the OCs. The bottom panels show the G , $G_{BP}-G_{RP}$ of GaiaDR2 stars for a 20 arcmin field region which is centered on the OCs and the likely cluster members (filled dots). V , $(B-V)$ plots are also displayed for all cluster stars: 170 small dots, NGC 2323, and 155 small dots, NGC 2539, together with their likely members (filled dots) inside the blue circles.

For the likely members of our OCs, the uncertainties of proper motions and the parallaxes are less than 0.30 mas yr⁻¹ and 0.15 mas, respectively. These limits nearly remain within the uncertainties of the proper motion components of $\sigma_{\mu_\alpha} < 0.28$ mas yr⁻¹ and $\sigma_{\mu_\delta} < 0.24$ mas yr⁻¹, and the uncertainty $\sigma_\varpi < 0.16$ mas for $G < 18$ mag, which are reported by the Gaia Collaboration, Lindegren *et al.* (2018) (see their table B.1.).

The median proper motion components plus their equatorial coordinates, found from GaiaDR2 astrometric data for the likely members of our OCs are listed in the parentheses of Table 1. Having applied these proper motion criteria to our OCs, the numbers of the likely cluster members are now appropriate for determining the astrophysical parameters in CC and CMDs.

4. Astrophysical parameters

4.1 Reddenings and photometric metal abundances

The two colour $(U-B)$, $(B-V)$ diagrams of the probable members of NGC 2323 and NGC 2539 are displayed in Figs. 6 and 9. Note that there are 56 (NGC 2323) and 42 stars (NGC 2539) which have $(U-B)$ colour. It appears that NGC 2323 contains early-type stars, which are mostly members of young open clusters. By using 11 early type stars with $(U-B) < 0$ (Fig. 6), the mean interstellar reddening is estimated as $E(B-V) = 0.23 \pm 0.04$ from Q-technique of early-type stars. The reddened intrinsic-colour sequence of the Schmidt-Kaler (SK82) (blue curve) for this $E(B-V) = 0.23$ is fitted on the CC of NGC 2323. For this, we adopt the following relations of Johnson and Morgan (1953) : $Q = (U-B) - 0.72(B-V)$, and $(B-V)_0 = 0.332Q$. Here $E(U-B) =$

$0.72E(B-V) + 0.05E(B-V)^2$, $E(B-V) = (B-V) - (B-V)_0$ and $E(U-B) = (U-B) - (U-B)_0$. The interstellar reddening, $E(B-V)$ of NGC 2539 is derived from displacement of the intrinsic-colour sequences of dwarfs and red giants from Schmidt-Kaler (1982)(SK82) in the CC diagram (Fig. 9), until the best fit to the cluster members has been achieved: along the (U-B) axis by $0.72E(B-V) + 0.05E(B-V)^2$ and along the (B-V) axis by $E(B-V)$.

F-type stars on the CC plots of these two OCs show ultraviolet excess, $\delta(U-B)$ above Hyades main sequence (MS) (green dashed curve), which are quite valuable for determining photometric metal abundance, $[M/H]$. Here, $\delta(U-B) = (U-B)_{Hyades} - \langle(U-B)_0\rangle$. By shifting the Hyades main-sequence according to the $E(B-V)$'s (col. 2 of Table 6), a fit is applied to the F-type stars, the same as used to fit the RC/RG stars to the SK82 giant colours. The best fit of iso-metallicity curves as representative of the mean metal abundances of the two OCs are shown as red solid lines in CC diagrams (Figs. 6 and 9). The average $\langle(B-V)_0\rangle$, $\langle(U-B)_{Hyades}\rangle$, $\langle(U-B)_0\rangle$ colours (cols. 3–5 of Table 6) have been fixed as mean values from the distribution of the F-type stars in each cluster. By using these average values, the ultraviolet excesses, $\delta(U-B)$ have been measured, and normalized to $(B-V)_0 = 0.6$ via the data of Table 1A given by Sandage (1969). We use $[M/H] = +0.13(\pm 0.04) - 4.84(\pm 0.60)\delta_{0.6} - 7.93(\pm 2.24)\delta_{0.6}^2$, by Karataş & Schuster (2006) to estimate photometric metallicity values ($[M/H]$) of the two OCs. With the equation $Z = Z_\odot \cdot 10^{[M/H]}$, their $[M/H]$ values are converted into the heavy-element abundance mass fraction, Z . The solar metal content is adopted as $Z_\odot = 0.0152$. The mean values, $\delta(U-B)$, $\delta(U-B)_{0.6}$, $[M/H]$ and Z of the two OCs are listed in cols. 6–9 of Table 6.

The $E(B-V)$ values from extinction maps given by Schlegel *et al.* (1998) (SFD) (based on the IRAS 100-micrometer surface brightness converted to extinction) have been obtained from NASA EXTRAGALACTIC DATABASE (NED) as $E(B-V)_{SFD,\infty} = 0.713$ and 0.032 for NGC 2323 and NGC 2539, respectively. Taking into consideration their distances d (kpc) (Cols. 3 of Tables 7–8) and Galactic latitudes (Col. 5 of Table 1), the final reddening, $E(B-V)_{SFD}$, for a given star is reduced compared to the total reddening $E(B-V)(\ell, b)_\infty$ by a factor $\{1 - \exp[-d \sin |b|/H]\}$, given by Bahcall & Soneira (1980), where b , d , and H are the Galactic latitude, distance and scale-height. These reduced $E(B-V)_{SFD}$ values are 0.13 (NGC 2323) and 0.02 (NGC 2539). Here we adopted $H=125$ pc (Bonifacio *et al.* 2000).

4.2 Distance moduli, distances and ages

For the determination of distances and ages of the two OCs, we have used the PARSEC isochrones of Bressan *et al.* (2012) for Y values which correspond to Z . Here, $Y=0.2485+1.78Z$. The PARSEC isochrones of Bressan *et al.* (2012) are over-plotted in four CMD's: $V, (B-V)$, $V, (V-I)$, $V, (R-I)$, $G, (G_{BP}-G_{RP})$ (Figs. 7–8 and Figs. 10–11). The $E(V-I)$, $E(R-I)$ and $E(G_{BP}-G_{RP})$ colour excesses are converted from the relations $E(V-I) = 1.25E(B-V)$, $E(R-I) = 0.69E(B-V)$ (Dean *et al.* 1978, Mathis 1990 and Straizys 1995) and $E(G_{BP}-G_{RP}) = 0.775E(B-V)$ (Bragaglia *et al.* 2018). A visual extinction of $A_V = 3.1 \times E(B-V)$ is applied to the absolute visual magnitudes of the isochrones.

The PARSEC isochrones are first shifted both vertically and horizontally on the CMDs according to the interstellar reddening values of $E(B-V)$, $E(V-I)$, $E(R-I)$, and $E(G_{BP}-G_{RP})$. Then the PARSEC isochrones have been shifted vertically to obtain the best fit to the observed main sequence, as well as the RC sequence. This vertical shift gives the (true) distance modulus, $DM = (V_0 - M_V)$. The distance moduli ($V_0 - M_V$) and distances, d (kpc), for the two OCs are presented in Cols. 2–3 of Tables 7–8.

For the determination of the ages (A , $\log(A)$) of these OCs, the isochrones of PARSEC, selected according to their Z values, have been shifted both vertically and horizontally in the CMD's with the expression $M_V + 3.1E(B-V) + DM$, for the vertical displacement and $C_0(\lambda_1 - \lambda_2) + E(\lambda_1 - \lambda_2)$, for the horizontal, where λ denotes the wavelengths of the various passbands. Here C_0 means de-reddened colour index. Then the age of the isochrone is varied until a satisfactory fit to the data has been obtained through the observed main-sequence (MS), turn-off (TO), sub-giant (SG) and RG/RC sequences. The derived ages are given in Cols. 4–5 of Tables 7–8.

To appreciate the uncertainties of the distance moduli and ages, additional PARSEC isochrones have usually been over-plotted in each CMD. The best fit is shown by red solid line, whereas, the uncertainties are represented by gray solid lines. The photometric uncertainties of colour indices are indicated in bottom left of CC and CMD plots.

For comparisons with the literature, we have taken into consideration mostly those physical parameters given by our $(B-V)$ colour indices, because the astrophysical parameters of these OCs are mostly given, and best represented, in terms of the CMD: $V, (B-V)$ (Table 11).

Table 6. The reddenings (Column 2), and the mean values of $\langle(U-B)_{Hyades}\rangle$ of the Hyades reference line, $\langle(U-B)_0\rangle$ values, for $\langle(B-V)_0\rangle$ (Cols. 3–5) as set by the iso-abundance lines for F-type stars of the two OCs. The $\delta(U-B)$, $\delta_{0.6}$, $[M/H]$ and Z are given in Cols. 6–9 together their uncertainties.

Cluster	$E(B-V)$	$\langle(B-V)_0\rangle$	$\langle(U-B)_H\rangle$	$\langle(U-B)_0\rangle$	$\delta(U-B)$	$\delta_{0.6}$	$[M/H]$	Z
NGC 2323	0.23 ± 0.04	0.48	+0.01	-0.03	0.04	0.044 ± 0.03	-0.10 ± 0.11	0.012 ± 0.003
NGC 2539	0.02 ± 0.06	0.51	0.06	-0.03	0.03	0.031 ± 0.03	-0.31 ± 0.12	0.007 ± 0.003

Table 7. The derived fundamental astrophysical parameters of NGC 2323 four colour indices. Its reddening, metal and heavy element abundances are as the following. $E(B-V) = 0.23 \pm 0.04$, $[M/H] = -0.10 \pm 0.11$, $Z = 0.012 \pm 0.003$.

Colour	(V_0-M_V)	d (kpc)	log(A)	A (Gyr)
$(B-V)$	10.00 ± 0.10	1.00 ± 0.05	8.30 ± 0.10	0.20 ± 0.05
$(V-I)$	09.90 ± 0.15	0.96 ± 0.07	8.30 ± 0.15	0.20 ± 0.08
$(R-I)$	09.90 ± 0.15	0.96 ± 0.07	8.30 ± 0.15	0.20 ± 0.08
$(G_{BP}-G_{RP})$	09.80 ± 0.10	0.91 ± 0.04	8.35 ± 0.10	0.20 ± 0.06

5. Results

5.1 NGC 2323

From 11 early type stars with $(U-B) < 0.0$ in Fig. 6, the reddening $E(B-V) = 0.23 \pm 0.04$ of NGC 2323 is determined. As is seen from Table 11, this reddening value is quite consistent with the literature values, $E(B-V) = 0.20-0.28$, within the uncertainties. Our reddening value and the literature values are larger than $E(B-V)_{SFD} = 0.13$. NGC 2323's $\delta(U-B)_{0.6}$ gives the photometric abundance of $([M/H], Z) = (-0.10, 0.012)$ from the CC diagram (Fig. 6).

From the CMDs for the colour indices $(B-V)$, $(V-I)$, $(R-I)$ and $(G_{BP}-G_{RP})$ (Figs. 7–8), values for the distance moduli, distances, and ages together with their uncertainties for NGC 2323 are presented in Table 7. The 200 Myr PARSEC isochrone with $Z = 0.012$ fits well the main sequence for all colour indices. No evolved stars are seen in the CMDs of NGC 2323. The PARSEC isochrones fit well the evolutionary sequences, as is seen from the CMDs. We derived the distance modulus and distance as $(V_0-M_V, d(\text{kpc})) = (10.00 \pm 0.10, 1.00 \pm 0.05)$, by fitting the PARSEC isochrones to the $(V, (B-V))$ diagram (Fig. 7(a)). The differences with the literature are at a level of $\Delta(V_0-M_V) = 0-0.46$ mag and $\Delta d = 0-0.11$ kpc. Our age value is somewhat older than the age range of 100–140 Myr in the literature (Table 11). This is to be expected since we used $Z = 0.012$ instead of the solar metal abundance. The distance modulus and distance of this OC are in agreement with the literature values (Table 11). Note that some authors of the literature do not give their uncertainties.

Our CCD $UBV(RI)_{KC}$ photometric data of NGC

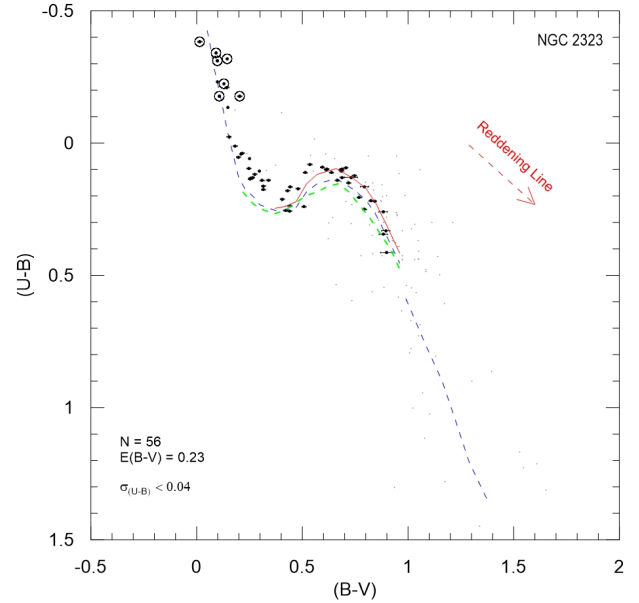


Figure 6. The reddened $(U-B, B-V)$ diagram for the likely members of NGC 2323. The blue dashed line shows the SK82 relation for both the main sequence (upper part) and the red giants (lower part). The green dashed line denotes the Hyades main-sequence. The fitted iso-metallicity line is indicated by the solid red curve. Grey dots indicate the non-members. The reddening vector is the dashed red arrow, and big circles indicate the seven definite members (See Table 10).

2323 contain seven definite early-type members, according to the SIMBAD data-base. The GaiaDR2 parallaxes/distances plus UBV photometry of these seven definite members are listed in the top rows of Table 10. These are also marked as big circles in the CC and CMDs (Fig. 6 and Figs. 7–8). Our photometric distances of $(B-V)$, $(V-I)$, $(R-I)$, and $(G_{BP}-G_{RP})$ provide good agreement with the Gaia DR2 distances (Col. 7, Table 10) within their uncertainties.

5.2 NGC 2539

A reddening value, $E(B-V) = 0.02 \pm 0.06$ for NGC 2539 (Fig. 9) is derived. Within the uncertainties, this value is in good coherent with the ones of the literature (Table 11). The reduced $E(B-V)_{SFD} = 0.02$

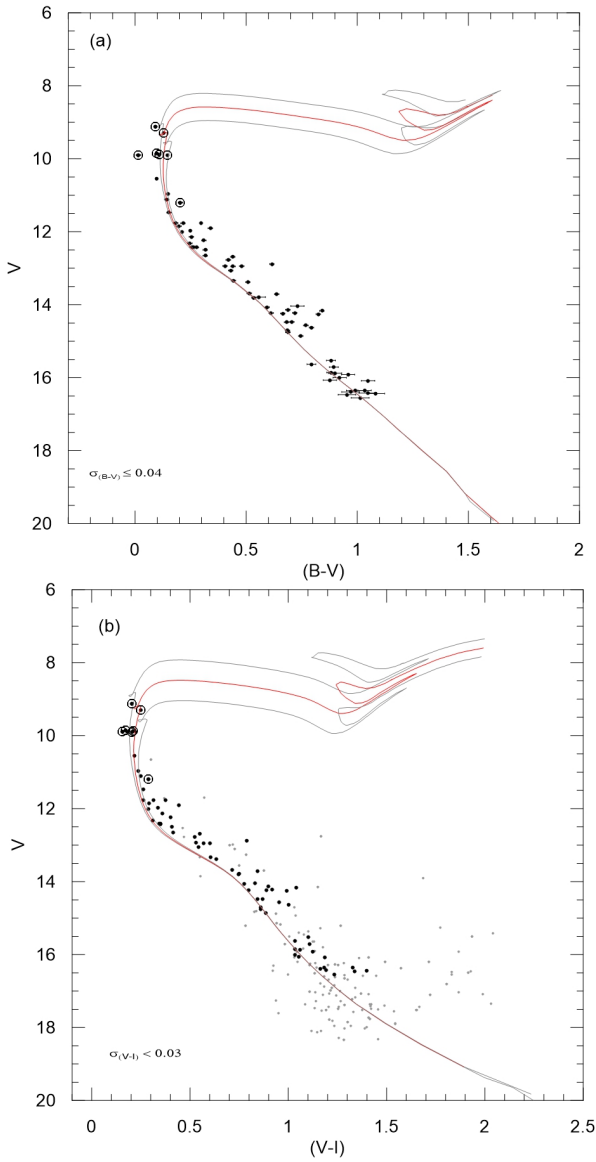


Figure 7. For NGC 2323, CMDs of $(V, B-V)$ (panel a) and $(V, V-I)$ (panel b). Red curves show the PARSEC isochrones interpolated to $Z = +0.012$. Solid grey isochrones have been drawn to provide a means for appreciating the uncertainties of the ages. Filled and grey dots indicate the members and non-members, respectively.

value for this OC is in good agreement with our reddening value. NGC 2539's $\delta(U-B)_{0.6}$ gives the photometric abundance of $([M/H], Z) = (-0.31, 0.007)$ from the CC diagram (Fig. 9).

The CMDs for the colour indices $(B-V)$, $(V-I)$, $(R-I)$, $(G_{BP}-G_{RP})$ of NGC 2539 are presented in panels (a)–(b) of Figs. 10–11. The isochrone with $Z = 0.007$ fits well the main sequence for all colour indices. The derived fundamental parameters together with their uncertainties from these CMDs have been given in Table 8. For the $(B-V)$ colour, our values

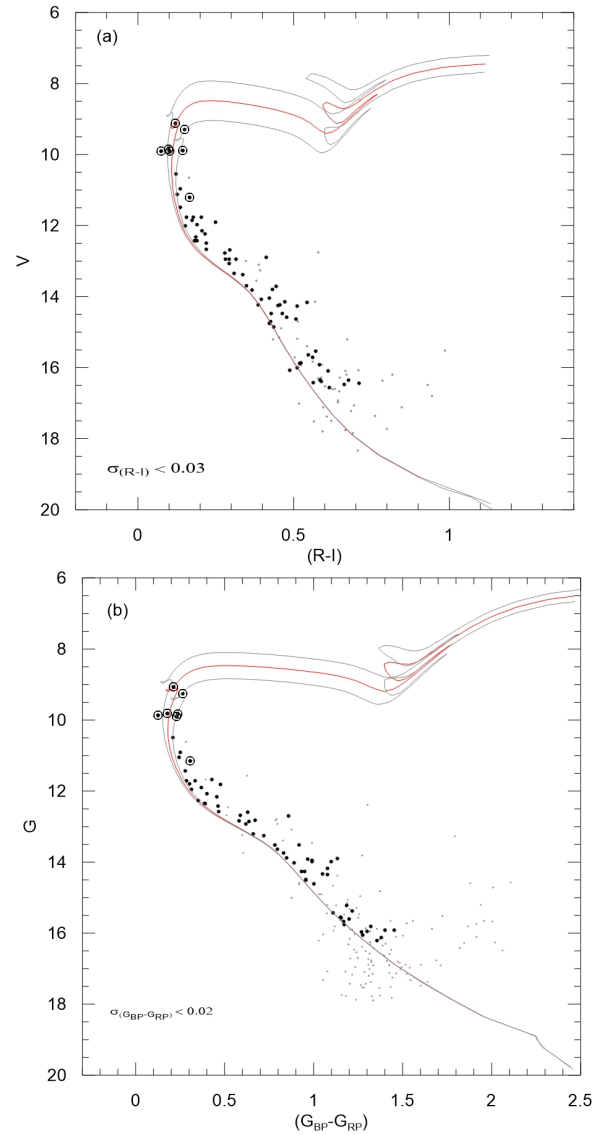


Figure 8. For NGC 2323, CMDs of $(V, R-I)$ (panel a) and $(G, G_{BP}-G_{RP})$ (panel b). The symbols are the same as Fig. 7.

Table 8. The derived fundamental astrophysical parameters of NGC 2539 four colour indices. Its reddening, metal and heavy element abundances are as the following. $E(B-V) = 0.02 \pm 0.06$, $[M/H] = -0.31 \pm 0.12$, $Z = 0.007 \pm 0.003$.

Colour	$(V_0 - M_V)$	d (kpc)	$\log(A)$	A (Gyr)
$(B-V)$	10.00 ± 0.04	1.00 ± 0.02	8.95 ± 0.05	0.89 ± 0.11
$(V-I)$	10.00 ± 0.10	1.00 ± 0.05	8.95 ± 0.10	0.89 ± 0.23
$(R-I)$	10.00 ± 0.10	1.00 ± 0.05	8.95 ± 0.10	0.89 ± 0.23
$(G_{BP}-G_{RP})$	10.10 ± 0.10	1.00 ± 0.05	8.95 ± 0.10	0.89 ± 0.23

$(V_0 - M_V) = 10.00 \pm 0.04$ and $d(\text{kpc}) = 1.00 \pm 0.02$ are in good concordance with the ones of the literature within the uncertainties (Table 11). The differences with the literature for NGC 2539 are at a level of $\Delta(V_0 - M_V) = 0.10 - 0.50$ mag and $\Delta d = 0.05 - 0.29$ kpc. Our age value 0.89 ± 0.11 Gyr (890 Myr) for NGC 2539

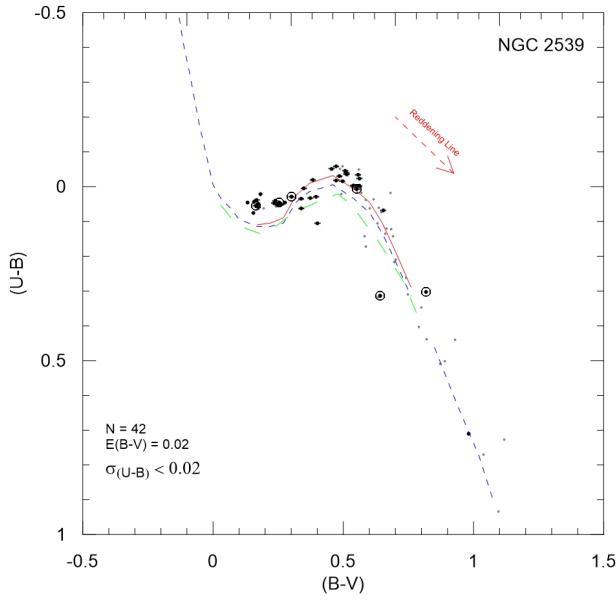


Figure 9. The reddened $(U-B, B-V)$ diagram for NGC 2539. The six definite members are shown as circles. The meanings of the symbols are the same as Fig. 6

seems to be slightly older than the age range of 540–640 Myr of the literature (Table 11).

No RC/RG candidates are detected in the CMDs of NGC 2323 because of its younger age ($A = 0.20$ Gyr). Note that the possible RC/RG candidates in the CMDs of NGC 2539 (square dots, Figs. 10–11). One of them is named BD-12 2380, according to the SIMBAD database. One can expect to detect this possible RC/RG star in the central part of NGC 2539, depending on its age ($A = 0.89$ Gyr). For the this giant candidate, from the $V, (B-V)$ and $V, (V-I)$ CM diagrams (square dot, panels (a)–(b) of Fig. 10), we have utilised the distance criteria for its membership as a initial test. In the case of the possible RG candidates, the RG candidates will not necessarily give the right distances to these clusters since their apparent magnitudes will depend on their position along the RG branch.

For the case of a possible RC candidate, its distances have been estimated from the mean absolute magnitudes of $\langle M_V \rangle = +0.60 \pm 0.10$, (Twarog *et al.* 1997) and $\langle M_I \rangle = -0.22 \pm 0.03$ (Groenwegen 2008), and listed in Table 9 together with its equatorial coordinates plus its magnitudes of I and V . For the estimates, the total absorption relations of $A_V = 3.1 E(B-V)$ and $A_I = 1.98 E(B-V)$ (Gim *et al.* 1998), are included, with the $E(B-V) = 0.02$ value of NGC 2539. The magnitudes of I and V in Columns 3–4 of Table 9 are used for estimating the d_I and d_V distances. These distances are estimated as $d_I = 0.95 \pm 0.05$ kpc and $d_V = 0.91 \pm 0.09$ kpc. The giant candidates within $1-\sigma$ agreement of the uncertainties of d_I and d_V from the main-sequence fit-

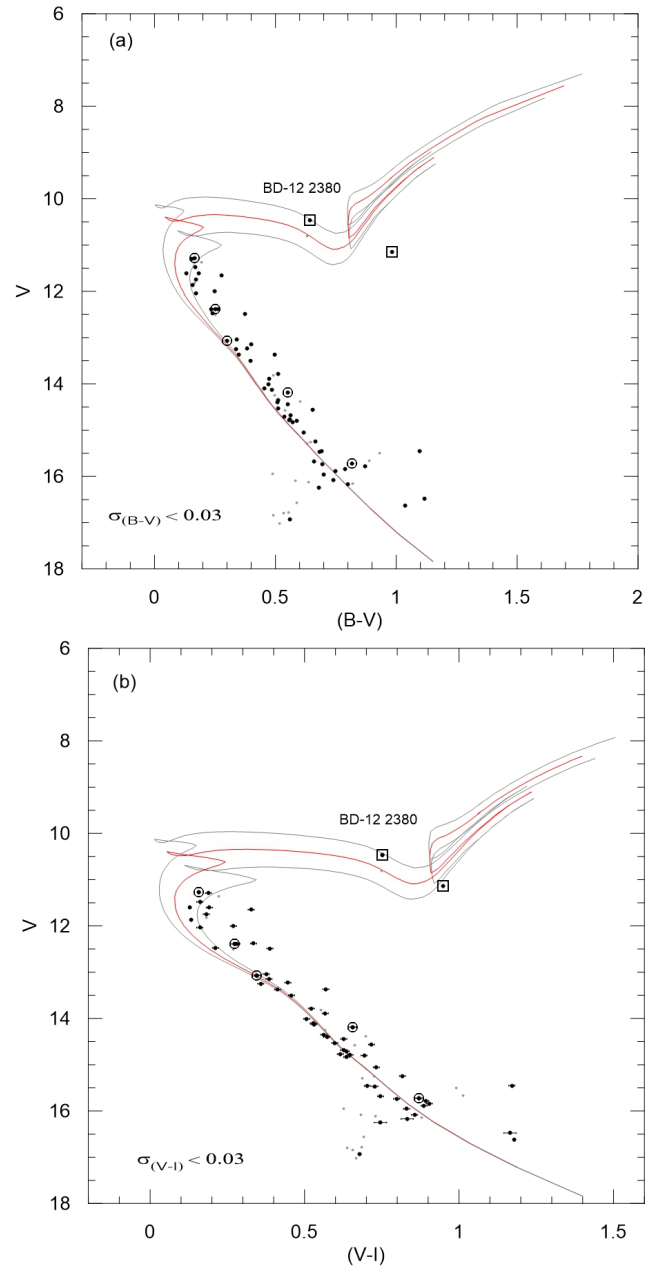


Figure 10. For NGC 2539, CMDs of $(V, B-V)$ (panel a) and $(V, V-I)$ (panel b). Red curves show the PARSEC isochrones interpolated to $Z = +0.007$. Solid grey isochrones have been drawn to provide a means for appreciating the uncertainties of the ages. Big open circles mark six definite members. Note that the two giant members (square dots) with $(V, B-V) = (10.462, 0.642)$ (BD-12 2380) and $(V, B-V) = (11.144, 0.982)$.

ting (Table 8) have been assigned as members, “M”, otherwise as non-members “NM” (Columns 7–8 of Table 9). The giant star, BD-12 2380 which fulfills both the d_I and d_V distances within its uncertainties is a definite member of NGC 2539. Its GaiaDR2 distance, $d = 1.20 \pm 0.07$ kpc ($\varpi = 0.833 \pm 0.047$) mas is close

to the photometric distances of Tables 8–9.

The other giant candidate does not seem to be RC candidate due to its location, $(V, B-V) = (11.144, 0.982)$ in the CMDs (square dot, Figs.10–11). Its GaiaDR2 distance $d = 1370 \pm 80$ pc ($\varpi = 0.732 \pm 0.041$ mas) is not close to the photometric distance, 1000 pc of Table 8.

From TO and RC/RC sequences on the CMDs of NGC 2539, for BD-12 2380 RC/RC candidate, we have determined its morphological age index (MAI).

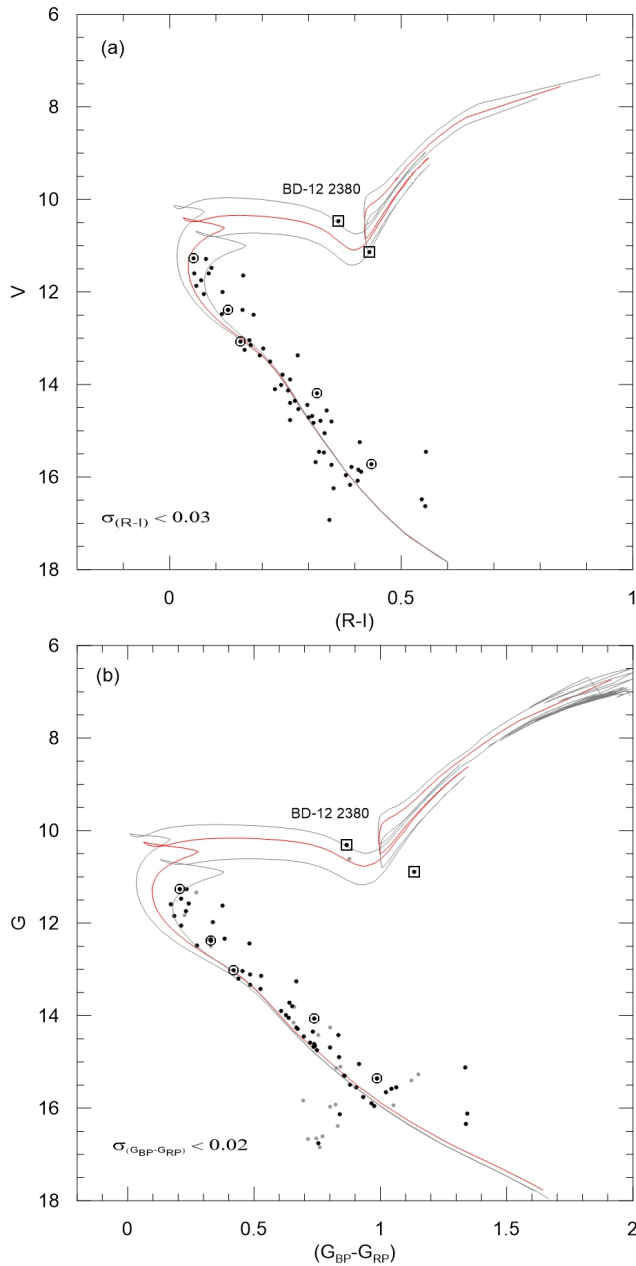


Figure 11. For NGC 2539, CMDs of $(V, R-I)$ (panel a) and $(G, G_{BP}-G_{RP})$ (panel b). The meanings of the symbols are the same as Fig. 10.

Table 9. First two rows show the membership test according to the distance criterion for the possible Red Clump (RC) member of NGC 2539. RA, DEC (Cols.1-2), VI photometry (Cols. 3-4), Distances for I and V magnitudes (Cols. 5-6), test distances (Cols. 7-8). “M” in Cols. 7–8 means member. The morphological age indices (MAI) of NGC 2539 are given at the bottom. “TO” and “RC” mean Turn-Off and Red Clump stars, respectively. The morphological age values, $\log A$ and A (Gyr) are listed in Cols. 7–8.

RA	DEC	I	V	d_I (kpc)	d_V (kpc)	d_I (test)	d_V (test)
122.71	-12.88	9.71	10.462	0.95 ± 0.05	0.91 ± 0.09	M	M
122.64	-12.86	10.20	11.144	0.96 ± 0.06	1.23 ± 0.14	M	NM

V_{TO}	V_{RC}	$(B-V)_{TO}$	$(B-V)_{RC}$	δV	δI	$\log A$	A (Gyr)
11.40	10.70	0.08	0.89	0.73	0.81	9.04 ± 0.05	1.09 ± 0.27

For this, δV and δI indices given by Phelps *et al.* (1994) are determined within its CMDs. Here, δV is the magnitude difference between the TO and RC stars, $\delta V = V_{TO} - V_{RC}$, and δI is the difference in the colour indices between the bluest point on the main sequence at the luminosity of the TO and the colour at the base of RG branch one magnitude brighter than the TO luminosity, $\delta I = (B-V)_{TO} - (B-V)_{RG}$. We measured the values of δI from its RC candidate, and then converted into δV by means of the equation of $\delta V = 3.77 - 3.75\delta I$ of Phelps *et al.* (1994). The photometric values obtained are listed at bottom of Table 9. With the aid of its photometric metal abundance, its morphological age is determined from the equation, $\log A = 0.04\delta V^2 + 0.34\delta V + 0.07[Fe/H] + 8.76$ of Salaris *et al.* (2004). The estimated MAI age is listed in the bottom line of Table 9 (Cols. 7–8) together with its uncertainty. The age difference between the MAI and isochrone techniques is $\Delta \log A = 0.09$ ($\Delta A = 0.20$ Gyr). These quite small differences indicate good consistency between the techniques.

The GaiaDR2 parallaxes/distances plus UBV photometry of six definite members which belong to NGC 2539, according to SIMBAD-database are listed in the bottom rows of Table 10. Differences fall in the range of $\Delta d = 200$ –456 pc between the 1000 pc value of all colours (Table 8) and the ones of GaiaDR2 (Col. 7; Table 10). In the sense their distances of these six definite members are not close to the photometric distances of NGC 2539 of four colour indices within the uncertainties.

6. Discussions and Conclusions

The reddenings of $E(B-V) = 0.23 \pm 0.04$ of NGC 2323 and $E(B-V) = 0.02 \pm 0.06$ of NGC 2539 are quite

Table 10. Our *UBV* photometry and Gaia DR2 parallaxes for the definite members of NGC 2323 (seven) and NGC 2539 (six), according to the SIMBAD data-base. Star designations (Cols. 1–2), *V*, (*U*–*B*), (*B*–*V*) (Cols. 3–5). GaiaDR2 parallaxes (mas) and their converted distances (pc) together with the uncertainties (Cols. 6–7).

Star-ID	Star No	<i>V</i>	(<i>U</i> – <i>B</i>)	(<i>B</i> – <i>V</i>)	$\varpi \pm \sigma_\varpi$	$d \pm \sigma_d$
NGC 2323						
228	HD 52965	9.13	-0.34	0.09	1.004±0.042	996±42
163	BD-08 1703	9.30	-0.22	0.13	1.170±0.045	855±33
256	BD-08 1700	9.85	-0.31	0.10	0.914±0.047	1094±56
402	BD-08 1695	9.88	-0.18	0.11	0.967±0.046	1034±49
359	BD-08 1696	9.90	-0.38	0.02	1.008±0.047	992±46
70	BD-08 1708	9.90	-0.32	0.14	0.951±0.060	1052±66
105	HD 52980B	11.20	-0.18	0.20	1.023±0.041	978±39
NGC 2539						
37	BD-12 2380	10.46	0.31	0.64	0.833±0.047	1200±70
168	BD-12 2373	11.28	0.06	0.16	0.713±0.063	1403±120
234	V0691Pup	12.39	0.05	0.25	0.796±0.048	1256±80
122	V0693Pup	13.07	0.03	0.30	0.782±0.038	1279±60
98	V0694Pup	14.18	0.01	0.55	0.687±0.034	1456±70
79	V0695Pup	15.72	0.30	0.82	0.730±0.050	1370±90

consistent with the ones of the literature (Table 11). The reddening differences with the literature are at a level of 0.00–0.05 for NGC 2323 and 0.04–0.08 for NGC 2539. For the (*B*–*V*) colour, distance moduli and distances of NGC 2323 and NGC 2539 are ($V_0 - M_V$, d (pc)) = (10.00±0.10, 1000±50) and ($V_0 - M_V$, d (pc)) = (10.00±0.04, 1000±20), respectively. The differences with the literature, derived using the (*B*–*V*) colour, are at a level of $\Delta(V_0 - M_V) = 0.00 - 0.46$ mag and Δd (kpc) = 0.00–0.11 for NGC 2323. These differences for NGC 2539 are at a level of $\Delta(V_0 - M_V) = 0.10 - 0.50$ mag and Δd (kpc) = 0.05–0.29. In the sense our detections are in good concordance with the values of the literature within the uncertainties (Table 11). For four colour indices (Tables 7–8), the values of ($V_0 - M_V$, d (kpc)) are 9.80–10.00 and 0.91–1.00 kpc for NGC 2323, and 10.00 and 1.00 kpc for NGC 2539, respectively, which are in agreement with each other and the literature values (Table 11).

The median GaiaDR2 parallax ($\varpi=0.998\pm0.136$ mas) of NGC 2323 (74 likely members) provides $d = 1000 \pm 140$ pc. This value is also similar to the photometric ones ($d = 910$ – 1000 pc) (Table 7), and also in good agreement with the distances of the literature (Table 11). For NGC 2539 (N=67 likely members), the median GaiaDR2 parallax $\varpi=0.751\pm0.139$ mas measures $d = 1330 \pm 250$ pc, which is reasonably close to our 1000 pc value (Table 8) within the uncertainties. For NGC 2539, the literature values are not as close to each other: $\varpi = 0.91$ mas ($d = 1.10$ kpc) and $\varpi = 0.78$ mas ($d = 1.29$ kpc). Our median parallaxes are similar to the values 0.997 ± 0.057 mas (NGC 2323) and 0.754 ± 0.064 mas (NGC 2539) of Cantat-Gaudin *et al.*

(2018) (Table 11).

Our age value (200 ± 50 Myr) of NGC 2323 is somewhat older than the age range of 100–140 Myr in the literature (Table 11). This occurs because we estimated $Z = 0.012$ from the ultraviolet excess (Fig. 6), instead of assuming the solar metal abundance. Likewise our estimated age, 890 ± 110 Myr for NGC 2539 is somewhat older than the age range 540–640 Myr of the literature (Table 11). The works of Joshi & Sagar (1986), Claria & Lapasset (1986), Choo *et al.* (2003) and Lapasset (2000) use different isochrones (Col. 8 of Table 11), and the differences in ages with respect to our values result from their usage of solar/different Z abundances with these isochrones. This work uses the $Z = 0.007$ abundance, which has been obtained from the $\delta(U-B)_{0.6}$ value of Fig. 9. The morphological age of NGC 2539 (the MAI method) of the one probable RC star (Table 9) has been determined as 1.09 ± 0.27 Gyr. This MAI age is quite compatible with its isochrone age (0.89 Gyr; Table 8).

The giant star, BD-12 2380 appears to be a definite member of NGC 2539 (square dot, Figs. 10–11) since the distances of $d_I = 950\pm50$ pc and $d_V = 910\pm90$ pc for *VI* filters (Table 9) are in harmony with the photometric distance 1000 ± 20 pc (Table 8) within the uncertainties. However, its GaiaDR2 distance $d = 1200 \pm 70$ pc ($\varpi = 0.833\pm0.047$ mas) is not close to the photometric distance of NGC 2539. The other giant candidate’s GaiaDR2 distance is $d = 1370 \pm 80$ pc ($\varpi = 0.732\pm0.041$ mas) but is not close to the photometric distance of NGC 2539. In the sense this may be a field giant. For further confirmation of its membership, spectroscopic observations are needed.

Acknowledgments

The observations of this publication were made at the National Astronomical Observatory, San Pedro Mártir, Baja California, México, and we wish to thank the staff of the observatory for their assistance during these observations. We thank H.Cakmak for useful helps on the manuscript. This research made use of the WEBDA open-cluster database of J.-C. Mermilliod; also the SIMBAD data-base. This work has been supported by the CONACyT (México) projects 33940, 45014, and 49434, and PAPIIT-UNAM (México) projects IN111500 and IN103014. This paper has made use of results from the European Space Agency (ESA) space mission Gaia, the data from which were processed by the Gaia Data Processing and Analysis Consortium (DPAC). Funding for the DPAC has been provided by national institutions, in particular the institutions participating in the Gaia Multilateral Agreement. The Gaia

Table 11. Comparison with the literature for our sample of OCs. The comparison is given here for our ($B-V$) results.

Cluster	E($B-V$)	(V_0-M_V)	d(kpc)	Age (Myr)	log A	Z	Isochrone	Photometry	Ref.
NGC 2323	0.23±0.04	10.00±0.10	1.00±0.05	200±50	8.30	0.012	Bressan et al.(2012)	CCD UBVR	This work
	0.23±0.06	10.00±0.15	1.00±0.07	140±20	8.15	solar	Yi et al. (2001);	UBV; CFHT	1
	-	-	-	115±20	8.06	solar	Bressan et al.(2012)	UBV; CFHT	1
	0.23	-	0.895	100	8.00	-	-	-	2
	0.25	9.85	1.00	140	8.15	0.019	Girardi et al.(2000)	Various broadband photometries	3
	0.28	10.46	1.107±0.07	-	8.30	0.019	Girardi et al.(2002)	2MASS JHK _s	4
	0.20	10.50	0.95	100	8.00	0.020	Bertelli et al.(1994)	CCD UBV	5
	0.22	10.00±0.17	1.00±0.08	130	-	0.020	Ventura et al.(1998)	BV with CFHT12Mosaic camera	6
	0.25±0.05	9.86	0.94	100±20	8.00	0.020	Bertelli et al.(1994)	Photoelectric UBV	7
	0.257	-	-	-	-	-	-	Stromgren	8
-	-	-	0.997±0.057	-	-	-	-	GaiaDR2 astrometry	9
NGC 2539	0.02±0.06	10.00±0.04	1.00±0.02	890±110	8.95	0.007	Bressan et al.(2012)	CCD UBVR	This work
	0.06±0.03	10.20±0.10	1.10±0.05	630	8.80	0.019	Girardi et al.(2000)	CCD UBVI	10
	0.06	10.42	1.21	630	8.80	0.020	Schaller et al.(1992)	photoelectric UBV	11
	0.08±0.02	10.10±0.30	1.05±0.15	540	8.73	0.030	Hejlesen (1980)	photoelectric UBV	12
	0.08±0.02	09.80±0.50	0.91±0.21	640±80	8.81	0.016	Mermilliod (1981)	CCD DDO, CMT ₁ T ₂ , UBV	13
	0.10±0.05	10.50±0.50	1.29±0.29	-	-	-	-	photoelectric UBV	14
	-	-	0.754±0.064	-	-	-	-	GaiaDR2 astrometry	9
	-	-	-	-	-	-	-	-	-

Table Notes. (1):Cummings, J et al. (2016), AJ, 818, 84; (2):Paunzen & Netopil (2014); (3): Frolov, V. N. et al. Ast. Lettr., (2012), 38,74; (4): Bukowiecki, L. et al. (2011), Acta Astronomica, 61, 231; (5): Sharma, S. et.al. (2006), AJ, 132, 1669; (6): Kalirai, J.S. et.al. (2003), AJ, 126, 1402 ;(7):Claria, J.J. et.al. (1998), A&ASS, 128, 131;(8):Schneider, H., (1987), A&ASS, 71, 531; (9): Cantat-Gaudin, T. et.al. (2018), Astronomy and Astrophysics, 618, 93; (10):Choo, K.J. et.al. (2003), A&A, 399, 99; (11):Lapasset, E. et.al. (2000), A&A, 361, 945 ;(12):Joshi&Sagar, (1986), Bull.Astr. Soc. India, 14, 95; (13):Claria&Lapasset (1986), ApJ, 302, 656; (14):Pesch (1961), ApJ, 134, 602.

mission website is <http://www.cosmos.esa.int/gaia>.

References

- Akkaya İ., Schuster W. J., Michel R., Chavarría-K C., Moitinho A., Vázquez R. and Karataş Y., 2010, *Rew Mex*, 46, 385 (A10)
- Akkaya Oralhan, I., Karataş, Y., Schuster,W.J., Michel, R., and Chavarría C., 2015, *New Astron.*, 34, 195 (A15)
- Bahcall, J.N., and Soneira, R.M., 1980, *Astrophys. J.*, 238, 17
- Bertelli, G., Bressan, A., Chiosi, C., Fagotto, F., and Nasi,E. 1994, *Astron. Astrophys. Suppl.*, 106, 275
- Bonifacio, P., Monai, S., and Beers, T. C. 2000, *Astron. J.*, 120, 2065
- Bragaglia, A., Fu, X., Mucciarelli, A., Andreuzzi, G., Donati, P. 2018, *Astron. Astrophys.*, 619, 176
- Bressan A., Marigo, P., Girardi L., Salasnich, B., Dal Cero, C., Rubele, S., Nanni, A., 2012, *Mon. Not. Roy. Astron. Soc.*, 427, 127
- Bukowiecki Ł., Maciejewski, G., Konorski, P., Strobel, A., 2011, *Acta Astron.*, 61, 231
- Caetano, T.C., Dias, W.S., Lépine, Monteiro, H.S., Moitinho, A., Hickel, G.R., Oliveira, A.F., 2015, *New Astron.*, 38, 31
- Cantat-Gaudin, T., Jordi, C., Vallenari, A., Bragaglia, A., Balaguer-Nunez, L., Soubiran, C., Bossini, D., Moitinho, A., Castro-Ginard, A., Krone-Martins, A., and 3 coauthors., 2018, *Astron. Astrophys.*, 618, 93
- Cardelli, J.A., Clayton G.C., Mathis, J.S., 1989, *Astrophys. J.*, 345, 245
- Choo, K. J., Kim, S.-L., Yoon, T. S., Chun, M.-Y., Sung, H., Park, B.-G., Ann, H. B., Lee, M. G., Jeon, Y.-B., Yuk, I.-S., 2003, *Astron. Astrophys.*, 399, 99
- Claria, J. J., Lapasset, E., 1986, *Astrophys. J.*, 302, 656
- Claria, J. J., Piatti, A. E., Lapasset, E., 1998, *Astron. Astrophys. Suppl.*, 128, 131
- Cummings, J.D., Kalirai, J.S., Tremblay, P.-E., Ramirez-Ruiz, E., 2016, *Astrophys. J.*, 818, 84
- Cutri, R., *et al.* , 2003, *2MASS All-Sky Catalogue of Point Sources*, CDS/ADC Electronic Catalogues 224
- Cutri, R.M. *et al.* , 2013, *yCat*, 2328, 0C.
- Dean, J.F., Warren, P.R., Cousins, A.W.J., 1978, *Mon. Not. Roy. Astron. Soc.*, 183, 569
- Dias, W.S., Alessi, B.S., Moitinho, A., Lépine J.R.D., 2002, *Astron. Astrophys.*, 389, 871
- Frolov, V. N., Ananjevskaja, Yu. K., Polyakov, E. V., 2012, *AstL*, 38, 74F
- Gaia Collaboration: Brown,A.G.A, Vallenari, A., Prusti, T., de Bruijne, J.H.J., *et al.* , 2016, *Astron. Astrophys.*, 595, A2
- Gaia Collaboration: Brown, A. G. A., Vallenari, A., Prusti, T. *et al.* , 2018, *Astron. Astrophys.*, 616, 1G
- Gaia Collaboration: Lindegren, L., Hernandez, J., Bombrun, A., Klioner, S. *et al.* , 2018, *Astron. Astrophys.*, 616, A2

- Gim, M., Vandenberg, D.A., Stetson, P., Hesser, J., Zurek, D.R., 1998, *Pub. Astron. Soc. Pac.*, 110, 1318
- Girardi, L., Bressan, A., Bertelli, G., Chiosi, C., 2000, *Astron. Astrophys. Suppl.*, 141, 371
- Girardi, L., Bertelli, G., Bressan, A., Chiosi, C., Groenewegen, M. A. T., Marigo, P., Salasnich, B., Weiss, A., 2002, *Astron. Astrophys.*, 391, 195
- Groenewegen, M.A.T., 2008, *Astron. Astrophys.*, 488, 935
- Hejlesen, P. M., 1980, *Astron. Astrophys. Suppl.*, 39, 347
- Joshi, U. C., Sagar, R., 2002, *BASI*, 14, 95
- Johnson, H.L., Morgan, W.W., 1953, *Astrophys. J.*, 117, 313
- Kalirai, J.S., Fahlman G.G., Richer, H.B., Ventura, P., 2003, *Astron. J.*, 126, 1402
- Karataş, Y., Schuster W.J., 2006, *Mon. Not. Roy. Astron. Soc.*, 371, 1793
- Kharchenko, N.V., Piskunov, A.E., Schilbach, E., Röser, S., Scholz, R.D., 2013, *Astron. Astrophys.*, 558, 53
- Landolt, A.U., 2009, *Astron. J.*, 137, 4186
- Lapasset, E., Claria, J. J., Mermilliod, J.-C., 2000, *Astron. Astrophys.*, 361, 945
- Lynga, G., Computer Based catalogue of Open Cluster Data, 5th. Ed. (Strasbourg: CDS, 1987)
- Mathis, J. 1990, *ARA&A*, 28,37
- Mermilliod, J. C., 1981, *Astron. Astrophys. Suppl.*, 44, 467
- Moitinho, A., 2010, Star clusters: basic galactic building blocks, *Proceedings IAU Symposium No.266*, eds. R.de Grijs and J.R.D. Lepine
- Paunzen, E., Netopil, M., Maitzen, H. M., Pavlovski, K., Schnell, A., Zejda, M., 2014, *Astron. Astrophys.*, 564, 42
- Pesch, P., 1961, *Astrophys. J.*, 134, 602
- Phelps, R.L., Jane,s K.A., Montgomery, K.A., 1994, *Astron. J.*, 107, 1079
- Roeser, S., Demleitner, M., Schilbach, E., 2010, *Astron. J.*, 139, 2440
- Salaris, M., Weiss, A., Percival, S.M., 2004, *Astron. Astrophys.*, 414, 163
- Sandage, A., 1969, *Astrophys. J.*, 158, 1115
- Schaller, G., Shaerer, D., Meynet, G., Maeder, A., 1992, *Astron. Astrophys. Suppl.*, 96, 269
- Schlegel, D.J., Finkbeiner, D. P., and Davis, M., 1998, *Astrophys. J.*, 500, 525
- Schneider, H., 1987, *Astron. Astrophys. Suppl.*, 71, 531
- Schmidt-Kaler, Th. 1982, in *Landolt-Bornstein, Numerical Data and Functional Relationships in Science and Technology*, New Series, Group VI, Vol.2b, eds. K. Schaifers and H. H. Voigt (Berlin: Springer), p. 14 (SK82)
- Schuster, W. J., Michel, R., Dias, W., Tapia-Peralta, T., Vázquez, R., Macfarland J., Chavarría, C., Santos, C., and Moitinho, A. 2007, *Galaxy Evolution Across the Hubble Time*, eds. F. Combes and J. Palouš, *Proceedings of the International Astronomical Union, IAU Symposium No. 235*, (Cambridge, United Kingdom: Cambridge University Press), p. 331
- Sharma, S., Pandey, A. K., Ogura, K., Mito, H., Tarusawa, K., Sagar, R., 2006, *AJ*, 132, 1669
- Skrutskie, M.F., Cutri, R., Stiening, R., Weinberg, M.D., Schneider, S.E., Carpenter, J.M., Beichman, C., Capps, R., 2006, *Astron. J.*, 131, 1163
- Stetson P. B., 1987, *PASP*, 99, 191
- Straizys, V. 1995, *Multicolor Stellar Photometry, Astronomy and Astrophysics Series*, Vol. 15, ed. A. G. Pacholczyk (Tucson, Arizona: Pachart Pub. House)
- Tapia, M. T., Schuster, W. J., Michel, R., Chavarría-K, C., Dias, W. S., Vázquez, R., and Moitinho, A., 2010, *Mon. Not. Roy. Astron. Soc.*, 401, 621 (T10)
- Twarog, B.A., Ashman, K.M., Anthony-Twarog, B.J., 1997, *Astron. J.*, 114, 2556
- van Dokkum P. G., 2001, *PASP*, 113, 1420
- Ventura, P., Zeppieri, A., Mazzitelli, I., & D'Antona, F., 1998, *Astron. Astrophys.*, 334, 953
- Yi, S., Demarque, P., Kim, Y.-C., Lee, Y.-W., Ree, C.H., Lejeune, T., Barnes, S., 2001, *Astrophys. J.*, 136, 417
- Zacharias, N., Finch, C.T., Girard, T.M. *et al.* , 2013, *Astron. J.*, 145, 44